ACS APPLIED MATERIALS & INTERFACES

Letter

Mesoporous Silica and Organosilica Nanomaterials as UV-blocking Agents

Nikola Knezevic, Nebojsa Ilic, Veljko R Djoki#, Rada Petrovic, and Djordje Janackovic

Just Accepted

ACS Publications

Mesoporous Silica and Organosilica Nanomaterials as UV-blocking Agents

Nikola Ž. Knežević,*[,†] Nebojša Ilić,[‡] Veljko Đokić,[‡] Rada Petrović,[‡] Đorđe Janaćković[‡]

[†]*BioSense Institute, University of Novi Sad, Dr Zorana Đinđića 1, Novi Sad 21000, Serbia,*

[‡]*Faculty of Technology and Metallurgy University of Belgrade, Karnegijeva 4, 11000 Belgrade, Serbia*

Abstract

Mesoporous silica nanoparticles (MSN) and periodic mesoporous organosilica nanoparticles containing bridging benzene (PMOBTB) and ethane (PMOBTE) moieties are synthesized, characterized and evaluated for application in skin protection from UVA/UVB sun irradiation. Furthermore, the influence of surface functionalization with chelating 3-(2-aminoethylamino)propylsilane and Zn^{2+} ions on the UV-blocking ability of MSN is evaluated, along with the photostability and capability of the synthesized nanomaterials to carry avobenzone, a known UV-absorbing agent. The obtained results reveal promising characteristics of MSN and PMO materials with regard to their potential for sunscreen applications, which could be beneficial in terms of alleviating concerns about health and environmental hazards of sunscreen ingredients.

Keywords:

Mesoporous silica nanoparticles, periodic mesoporous organosilica, sunscreen nanoparticles, UV protection, functionalized nanoparticles, application of nanoparticles

1

Different types of silica nanomaterials, typically classified as synthetic amorphous silica (SAS), can be found in the formulations since 1950s as reinforcement and thickening agents in various industries due to their high specific surface area and high water absorption capacity.[1] In cosmetic products, SAS materials are regarded as safe additives,[2] mostly used as abrasive, adsorbent, anticaking, bulking, opacifying and thickening agents. Currently applied sunscreen ingredients for active UVA and UVB protection of skin are predominantly ZnO and TiO_2 nanoparticles, which absorb, reflect and scatter UV radiation, along with organic molecules as UV absorbers e.g. avobenzone. However, there is an increasing concern regarding the adverse health and environmental effects of these sunscreen ingredients,[3-6] motivating researchers to find safer alternatives e.g. by coating the surface of hazardous nanomaterials with silica layers[7] or by encompassing organic UV absorbers within the framework of organosilica nanoparticles.[8] Recent *in vivo* study revealed that amine-functionalized silica nanoparticles of 55 nm in diameter did not penetrate the skin even in the case of disrupted skin structure,[9] which sustains the notion of their safety for application in skin products. However, particular attention needs to be taken into account during formulation of the SAS materials, as the skin penetration of silica nanoparticles increases in the case of formulation with skin penetration enhancers such as isopropyl myristate.[10]

Mesoporous silica nanoparticles (MSNs) have been demonstrated for a variety of applications since the beginning of the 21st century. This nanomaterial is characterized by its biocompatibility,[11] facile synthesis protocols,[12] possibilities for modifications of particle and pore sizes and morphologies,[13] a plethora of strategies for surface functionalization and modification of the nanomaterial's physico-chemical properties,[14] high surface area and thermal stability. Periodic mesoporous organic nanoparticles (PMO NPs) are more recently developed structural

2

analogues of MSNs, distinguished by the presence of bridging organic moieties within the silica framework.[15-17] Even though both types of porous SAS nanomaterials are thoroughly investigated for construction of multifunctional disease-targeting nanotherapeutics,[18] as well as in heterogeneous catalysis, separation and sensing, their application as UV-blocking agents, to the best of our knowledge, have not been characterized in the literature.

Herein we focused the study on evaluating the UV-blocking features of the porous silica nanomaterials with different constitution, i.e. MSN and PMO NPs with ethane and benzene bridges, PMOBTE and PMOBTB, respectively. These PMO materials were recently developed for promising biomedical applications.[19-20] The influence of surface functionalization on UV-blocking ability was also investigated by constructing material containing a chelating ligand ~~3-(2-aminoethylamino)propylsilane~~ N-[3-(trimethoxysilyl)propyl]ethylenediamine (DA) on the surface of MSN (DAMSN) and the material with coordinated Zn^{2+} on DAMSN (ZnDAMSN). Functionalization with zinc was conducted having in mind the necessity of these ions in various zinc containing enzymes, most notably superoxide dismutase, alkaline phosphatase, matrix metalloproteinase and zinc finger proteins, which have significant roles in skin wound repair, maintenance and protection against inflammation.[21] Finally, we tested the photostability of materials under sun-simulated lamp and the capability of the synthesized materials to adsorb avobenzone. Photodegradation products of avobenzone have been correlated with photoallergic and cytotoxic effects on skin.[22] However, research studies already showed that mesoporous silicates have the capability to inhibit photodegradation of sunscreen ingredients, as in the example of entrapping octyl methoxycinnamate inside the mesopores of MSN, which yielded in the enhanced sunscreen photostability and safety.[23]

The nanoparticulate materials were obtained by condensation of silica precursors in basic aqueous environment, in the presence of mesopore-templating surfactant cetyltrimethylammonium bromide. In case of MSN the silica precursor was tetraethoxysilane (TEOS), while for PMOBTE and PMOBTB the sole silica precursors were 1,4-bis(triethoxysilyl)ethane (BTE) and 1,4-bis(triethoxysilyl)benzene (BTB), respectively (Figure 1a). After washing the materials with copious amounts of water and ethanol, the surfactant was removed by calcination at 600 ˚C in case of MSN or by sonication in ammonium nitrate solution (6 g/L in ethanol) in case of PMO materials. The analysis of scanning electron miscroscopy (SEM) images (Figure 1a-c) showed that all prepared materials were composed of spherical nanoparticles, with particle diameters in the ranges 75 - 215 nm, 510 - 710 nm and 120 - 330 nm for MSN, PMOBTE and PMOBTB nanoparticles, respectively. Transmission electron microscopy (TEM) images of these materials are shown on Figures S1-S3, evidencing hexagonal arrangement of tubular mesopores for MSN material, while the porous nature of PMO materials is less perceptible due to smaller diameter of pores with non-uniform packing and lower contrast between the organic framework and empty pores in comparison to the SiO_2 framework in MSN. However, the porous nature of all synthesized materials is indicated by their high Brunauer–Emmett–Teller (BET) specific surface areas and calculated Barrett-Joyner-Halenda (BJH) average pore diameters of nitrogen adsorption analyses (Figure S4). The highest specific surface area was obtained for MSN material (1369 m^2/g) with BJH average pore diameter of 2.8 nm. Among the porous organosilica nanoparticles, PMOBTE showed higher specific surface area (778 m^2/g) with BJH average pore diameter of 2.2 nm, while PMOBTB exhibited specific surface area of 391 m^2/g with BJH average pore diameter of 13.6 nm. The BJH values are obtained experimentally for average pores in the material and often differ from the peaks which can be

4

seen on the BJH graph (Figure S4), as the peaks on BJH graph typically represent the most

predominant pore diameters. The value of average pore diameter is typically larger than the

predominant pore diameters because of the pore voids between the nanoparticles, which are taken

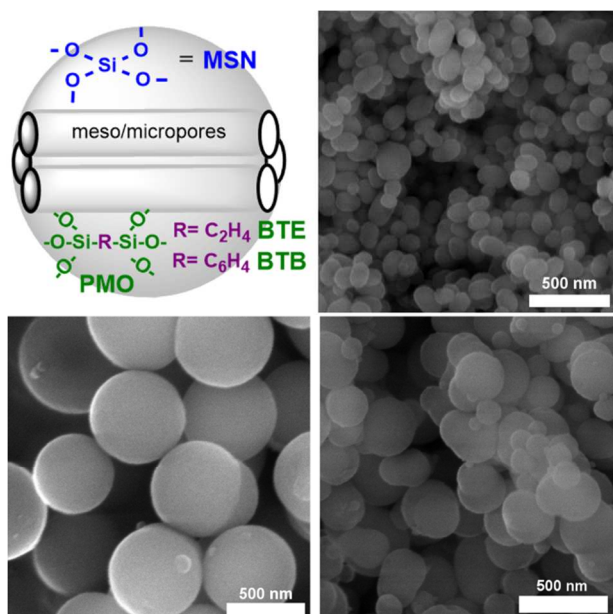into calculation during BJH analysis.

Figure 1. a) Schematic representation of the synthesized MSN and PMO NPs and representative

SEM images of MSN (b), PMOBTE (c) and PMOBTB (d).

Infrared spectroscopy confirms the composition of the synthesized nanoparticles (Figure 2).

Mesoporous silica nanoparticles are characterized by the strong overlapping Si-O vibrations in

the 1000-1250 cm^{-1} region. Peak at 1635 cm^{-1} and the broad band centered around 3400 cm^{-1} are

vibrations of the surface-adsorbed water. Upon functionalization of the silica surface, with (N-[3-

(trimethoxysilyl)propyl]ethylenediamine) DA in dry dimethylformamide at 110 ˚C, the new

bands appear in the spectrum of DAMSN at 2974 cm^{-1} and 2935 cm^{-1} due to CH(υ) vibrations,

5

1653 cm^{-1}, assigned to NH(δ) vibrations and CH bending vibrations at 1452 cm^{-1} and 1400 cm^{-1} (Figure 2a). The same bands appear in the IR spectrum of the material with Zn^{2+}-functionalized DAMSN (ZnDAMSN), with the additional sharp peak at 620 cm^{-1}, which indicates the presence of sulfate group on the nanoparticles upon reaction of ZnSO$_4$ with DAMSN in aqueous environment.[24] ~~The presence of Zn ions in ZnDAMSN was confirmed by electron absorption spectroscopy, which quantified Zn^{2+} in the amount of 0.5 wt% in the material.~~ The amount of functional groups on the DAMSN was 15.7 wt%, determined by the prominent weight loss in the range 200-530 °C from TGA measurement (Figure S5).[25] The weight loss at temperatures below 200 °C can be attributed to the surface-adsorbed water, while condensation of surface silanols occurs at temperatures around 600 °C.[26] In case of ZnDAMSN the weight loss peaks in TGA (Figure S6) shift to higher temperatures, indicating the binding to zinc ions, and the band overlap with the peaks for silanol condensation. The amount of Zn^{2+} in ZnDAMSN was determined by electron absorption spectroscopy in the amount of 0.5 wt%. These values also indicate that the molar ration of DA/Zn^{2+} is ca. 20, revealing that much of the surface-functionalized ligand remained non-coordinated, probably due to strong electrostatic interaction between amine moieties and deprotonated surface silanols, along with possible inaccessibility of ligands if functionalized deep inside the mesopores.

Comparison of the IR spectra of MSN, PMOBTE and PMOBTB is shown on Figure 2b. As expected, the PMO materials also exhibit the broad bands for different Si-O stretching vibrations in the material, as well as the peaks related to the surface adsorbed water as in the spectrum of MSN. In addition, PMOBTE material shows peaks from stretching CH vibrations at 2976 and 2922 cm^{-1} and the peaks from scissoring and rocking vibrations of the bridging CH$_2$ groups at 1412 and 1271 cm^{-1}, respectively. Both PMOBTE and PMOBTB exhibit Si-C stretching peaks at

6

1159 and 1155 cm^{-1}, respectively. The IR spectrum of PMOBTB additionally exhibits the peaks

arising from the bridging benzene moiety, i.e. stretching CH at 3062 and 3014 cm^{-1}, out of plane

CH bending vibrations at 924, 777 and 534 cm^{-1}, while the stretching C=C band is overlapping

with the vibration peak of adsorbed water at 1632 cm^{-1}.[27]
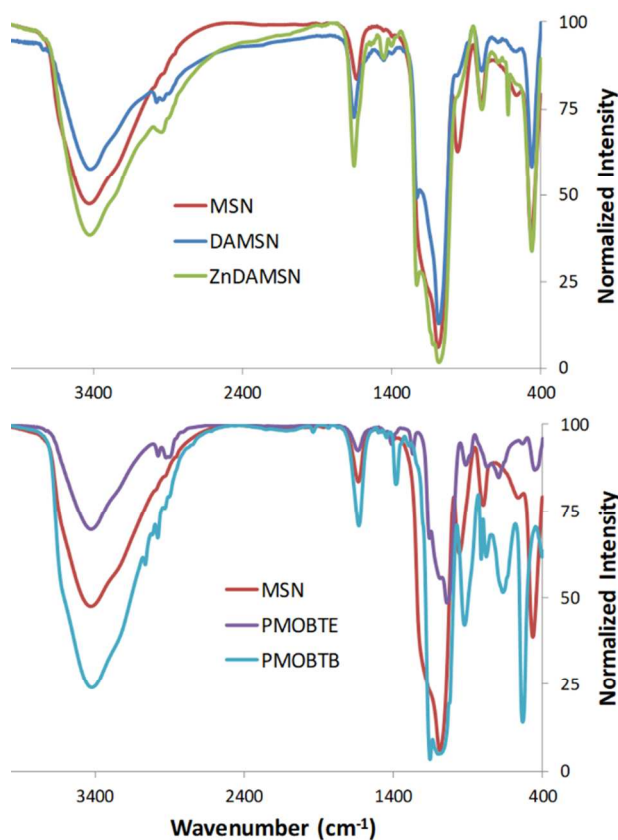
Figure 2. Infrared spectra of the synthesized materials: a) Comparison of IR spectra of MSN, DAMSN and ZnDAMSN; b) Comparison of MSN, PMOBTE and PMOBTB

The UV-blocking features of the materials were characterized by determination of sun protection

factor (SPF) values, the critical wavelength and UVA/UVB ratios. SPF is defined as the UV

energy required to produce a minimal erythemal dose (MED) on protected skin, divided by the

UV energy required to produce a MED on unprotected skin. MED is defined as the lowest time

7

interval or dosage of UV light irradiation sufficient to produce a minimal, perceptible erythema on unprotected skin.[28] Absorption spectroscopy has been shown as a simple methodology for characterization of UV-protection characteristics of materials, with thus calculated SPF values which can be reliably correlated to the in vivo determined SPF.[29,30] For the calculation of SPF values, the absorbance values at wavelengths of 290-320 were noted and SPF values were determined by employing the Mansur equation.[30]

$$SPF_{spectrophotometric} = CF \times \sum_{290}^{320} EE(\lambda) \times I(\lambda) \times Abs(\lambda)$$

Where CF is the correction factor (=10), EE (λ) erythemal effect spectrum, I (λ) solar intensity spectrum, Abs (λ) absorbance of the solution. The values of EE and I are constants, determined by Sayre et. Al.[31]

The critical wavelength and UVA/UVB ratios were also determined from the obtained UV/VIS spectra according to the established equations:[8]

$$\int_{290}^{\lambda c} A(\lambda) \, d\lambda = 0.9 \int_{290}^{400} A(\lambda) \, d\lambda$$

and

$$\frac{UVA}{UVB} \, ratio = \frac{\int_{320}^{400} A(\lambda)d\lambda / \int_{320}^{400} d\lambda}{\int_{290}^{320} A(\lambda)d\lambda / \int_{290}^{320} d\lambda}$$

where λc is the critical wavelength, A(λ) is the average absorbance at each wavelength, and dλ is the wavelength interval between measurements.

8

In case of the herein synthesized materials the calculated SPF values of both porous organosilica nanomaterials (PMOBTE and PMOBTB) are significantly higher than the SPF value of MSN, i.e. 9.1 and 18.5 vs. 1.2, respectively (Table 1), while surface functionalization of MSN increases the SPF values from 1.2 to 5.5 and 4.3 for DAMSN and ZnDAMSN, respectively.

Table 1. Spectrophotometric characterizations of the UV-blocking features of the materials

	MSN	DAMSN	ZnDAMSN	PMOBTE	PMOBTB
SPF	1.2 ± 0.1	5.5 ± 0.1	4.3 ± 0.2	9.1 ± 0.1	18.5 ± 0.2
λ(critical)	386 nm	386 nm	386 nm	388 nm	386 nm
UVA/UVB	0.74	0.79	0.78	0.90	0.78

To explain the obtained results of SPF calculations, dynamic light scattering (DLS) measurements on suspensions in ethanol of all prepared materials were performed (Figure 3). The average hydrodynamic diameters (from the three consecutive measurements) of the nanoparticles were 179 ± 23 nm, 224 ± 7 nm, 229 ± 13 nm, 541 ± 70 nm and 357 ± 17 nm for MSN, DAMNS, ZnDAMSN, PMOBTE and PMOBTB respectively.
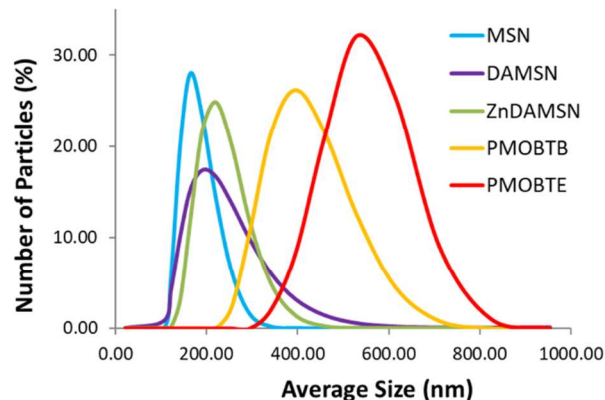

Figure 3. Hydrodynamic diameters of nanoparticles as determined by DLS measurements

Hence, the difference in SPF between the synthesized materials can be attributed to the differences in their capability to scatter light in the UVA (400-320 nm) and UVB region (320-290 nm). The highest SPF value was obtained for PMOBTB, which has the majority of particles in the perfect range for interaction with UVA and UVB light with the average DLS diameter of 357 nm. PMOBTE nanoparticles have much bigger average DLS diameter (541 nm), though a portion of the material shows DLS scattering in the UVA and UVB region as well. On the contrary, MSN nanoparticles are too small and show no evidence of light scattering in the region of interest for skin protection, and thus exhibit the small SPF value. However, upon surface functionalization of MSN with hydrophilic, charged moieties, the average hydrodynamic diameters increased from 179 nm (MSN) to 224 nm (DAMSN) and 229 nm (ZnDAMSN), and the DLS data evidence significant portion of light scattering in the UVA and UVB region. This extension of light scattering to higher wavelengths is probably a result of enhanced capability for dimerization and further agglomeration of individual nanoparticles in case of surface-functionalization with DA moiety, capable of $N \cdots H$ hydrogen bonding and attractive electrostatic interactions in the presence of Zn^{2+} and SO_4^{2-} ions in the case of ZnDAMSN. Hence, in addition to the beneficial effects of the presence of Zn^{2+} to the skin health, as discussed above, its functionalization on the surface also led to the enhanced sun-screening efficacy of the obtained material.

To investigate the influence of composition of nanoparticles on the UV-blocking ability we synthesized PMOBTB material with much smaller diameter (PMOBTB2, 114 ± 3 nm by DLS size measurements) (Figure S7-S9 for TEM, IR and DLS) and determined its UV blocking characteristics. Even though the size of these nanoparticles is even smaller than for MSN material, the light scattering/absorption in the UV region was evidently substantially bigger

10

(Figure S10), which can be ascribed to the presence of UV absorbing benzene bridges in their framework. Thus, the enhanced UV blocking ability of PMOBTB2 is evidenced by its high SPF of 10.4 ± 0.1. Evidently, the bigger diameter of nanoparticles of PMOBTB material still warrant higher UV-blocking ability with calculated SPF of 18.5, but the different composition of PMOBTB2 and MSN governs the significant differences in the SPF values, 10.5 vs 1.2 respectively, regardless of the smaller diameter of PMOBTB2. In addition, the difference in the intensities of UV/VIS spectra of the suspensions of PMOBTB2 and the same material without washing the surfactant template (PMOBTB2s, Figure S10) indicate the significance of porosity of the nanoparticles for their UV blocking efficacy. Indeed, higher porosity allows more light-scattering particles in the suspension per mass unit of the material due to its lower density. Hence, without washing out the surfactant the obtained SPF value of PMOBTB2s was 9.1 ± 0.1.

Critical wavelength (*λc*) is defined as the wavelength below which 90% of the total UV absorbance occurs.[30] The obtained UV/VIS absorbance data reveal that all synthesized materials have *λc* well above 370 nm (Table 1, for PMOBTB2 and PMOBTB2s *λc* = 383 nm), which classifies them as broad-spectrum (UVA + UVB) sunscreen agents. The ratios of mean UVA to UVB absorbances for all the materials were also calculated (Table 1, for PMOBTB2 = 0.82 and PMOBTB2s UVA/UVB = 0.56), and the results reveal that PMOBTE material has the highest capability for UVA protection, with the UVA/UVB ratio of 0.9, which is classified as maximum (***) UVA protection agent.[32] All other materials noted in Table 1 have the values slightly lower than 0.8 and would be characterized as superior (***) UVA blockers. Notably, PMOBTB2 material also shows maximum (****) UVA protection rating while UVA protection capability of PMOBTB2s is rated good (**).

11

Typical UV/VIS absorbance spectra of isopropanol suspensions of the synthesized materials and their stability upon irradiation with a sun-simulated lamp for 30 minutes are represented on Figure 4a. The spectrum of PMOBTB shows a characteristic broad band of the benzene moiety centered at 270 nm. The increasing UV-light scattering capabilities of the prepared materials in the order MSN<PMOBTE<PMOBTB is clearly evident from the provided spectra of the suspensions in the same mass concentrations. In addition, neither of the tested materials changed their UV/VIS absorbance spectra after exposure to irradiation, indicating their good photostability. As a comparison, irradiation of the solution of avobenzone in isopropanol with the same sun-simulating lamp (Figure 4b) led to lowering of absorbance of this typical sunscreen ingredient, demonstrating its instability upon exposure to light.
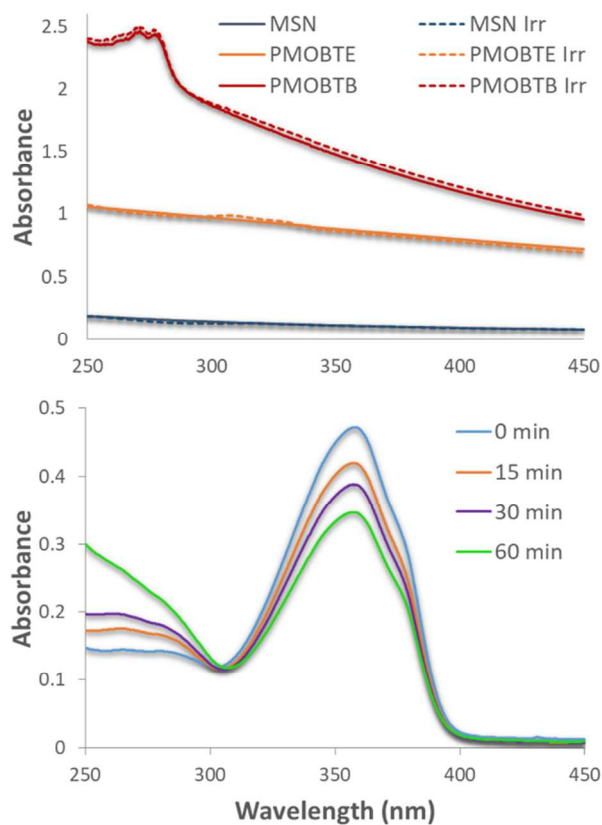
Figure 4. UV/VIS spectra of: a) MNS, PMOBTE and PMOBTB in isopropanol before and after exposure to sun-simulated irradiation for 30 minutes (Irr), b) avobenzone in isopropanol upon exposure to irradiation for different time periods.

The capability of the synthesized materials to adsorb and retain the avobenzone on their surface was also demonstrated as an additional benefit in utilization of these nanoparticulate materials for sunscreen applications. Different types of organic and inorganic sun-screening agents can be housed on the silica surface or retained inside their mesopores, which may improve the sun-screening characteristics of both the nanoparticles and the cargo agents, as well as to possibly decrease the health concerns of sunscreen ingredients if they are confined within the silica nanoparticles. The loading capacity of avobenzone in MSN was 0.9 mg/g, while for PMOBTE and PMOBTB was 1.1 mg/g, which were obtained even after copious washings of the material with isopropanol and ethanol.

Finally, we perceive that even though the calculations suggest that PMOBTB material should be chosen for formulation of sunscreens in case of the need for highest SPF and PMOBTE material for the sunscreens with the highest UVA protection, these materials would not be typically favored for commercial sunscreens due to their strong blocking of light in the visible spectrum, which would render the sunscreens non-transparent and thus less esthetically pleasing. Instead, other herein synthesized materials would be preferred, having the lower blocking of visible light. We presume that a good candidate for formulation of effective and safe sunscreens would be PMOBTB2 type of material, having high SPF, critical wavelength and UVA/UVB ratio, along with advantages in low visible light scattering and different possibilities for increasing the UV

13

protection capabilities through suitable surface modifications, which is to be confirmed by future studies.

In conclusion, porous silicon-based nanoparticles of different composition (silica or bridged organosilica), size and surface characteristics (nonfunctionalized, ethylenediamine- and Zn^{2+}-functionalized) were synthesized, characterized and their potentials for applications as UV-blocking agents were evaluated. Functionalization of the MSN surface led to enhancements of UVA and UVB blocking abilities of the materials, while PMO nanoparticulate materials showcased superior UV-screening characteristics over their MSN counterparts. Both particle size and their composition significantly influence their UV protection efficacy, with particles of ca. 350 nm in diameter and particles containing UV-absorbing benzene moieties in the framework showing the highest SPF values. All prepared materials can be classified as broad-spectrum sunscreen agents since the calculated critical wavelengths are well above 370 nm. The organosilica nanomaterial with ethane bridges (PMOBTE) showed the highest UVA/UVB ratio of 0.9, which, along with the value for PMOBTB2 materials (0.82), is considered as maximum (****) UVA protection. All other porous nanomaterials are characterized as superior (***) UVA protecting agents. The materials showed high stability toward photodegradation and the capability to adsorb avobenzone on their surface. This study reveals for the first time the high potential of functionalized MSN and PMO materials for application in skin protection from UV irradiation and opens the possibilities to replace the currently used ingredients in sunscreens with potentially more health- and environment-friendly silica-based materials.

Associated content

14

Supporting information

The Supporting Information is available free of charge on the ACS Publications website at DOI:

Experimental methods, TEM images of MSN, PMOBTE and PMOBTB (Figure S1-S3), BET and BJH graphs (Figure S4), TGA data for DAMSN and ZnDAMSN (Figures S5 and S6), characterization of PMOBTB2 material: TEM images (Figure S7), IR spectra of PMOBTB2s and PMOBTB2 (Figure S8), DLS measurements of PMOBTB2s and PMOBTB2 (Figure S9), UV/VIS spectra of suspensions of all synthesized materials at concentration of 0.2 mg/mL in ethanol (Figure S10).

Author information

Corresponding author: Nikola Knezevic, email: nknezevic@biosense.rs

ORCID

Nikola Knezevic: 0000-0002-1563-7763

Acknowledgements

15

References

(1)   Waddell, W. H.; Evans, L. R., Silica, Amorphous Silica. In *Kirk-Othmer Encyclopedia of Chemical Technology*, John Wiley & Sons, Inc.: 2000.

(2)   Sccs; Hoet, P. H. M., Opinion of the Scientific Committee on Consumer Safety (SCCS) – Revision of the opinion on the safety of the use of Silica, Hydrated Silica, and Silica Surface Modified with Alkyl Silylates (nano form) in cosmetic products. *Regul. Toxicol. Pharmacol.* **2016,** *74*, 79-80.

(3)   Xia, T.; Kovochich, M.; Liong, M.; Mädler, L.; Gilbert, B.; Shi, H.; Yeh, J. I.; Zink, J. I.; Nel, A. E., Comparison of the Mechanism of Toxicity of Zinc Oxide and Cerium Oxide Nanoparticles Based on Dissolution and Oxidative Stress Properties. *ACS Nano* **2008,** *2*, 2121-2134.

(4)   Grande, F.; Tucci, P., Titanium Dioxide Nanoparticles: a Risk for Human Health? *Mini-Rev. Med. Chem.* **2016,** *16*, 762-769.

(5)   Morabito, K.; Shapley, N. C.; Steeley, K. G.; Tripathi, A., Review of sunscreen and the emergence of non-conventional absorbers and their applications in ultraviolet protection. *Int. J. Cosmet. Sci.* **2011,** *33*, 385-390.

(6)   Sánchez-Quiles, D.; Tovar-Sánchez, A., Are sunscreens a new environmental risk associated with coastal tourism? *Environ. Int.* **2015,** *83*, 158-170.

(7)   Sotiriou, G. A.; Watson, C.; Murdaugh, K. M.; Darrah, T. H.; Pyrgiotakis, G.; Elder, A.; Brain, J. D.; Demokritou, P., Engineering safer-by-design silica-coated ZnO nanorods with reduced DNA damage potential. *Environ. Sci.: Nano* **2014,** *1*, 144-153.

(8)   Tolbert, S. H.; McFadden, P. D.; Loy, D. A., New Hybrid Organic/Inorganic Polysilsesquioxane–Silica Particles as Sunscreens. *ACS Appl. Mater. Interfaces* **2016,** *8*, 3160-3174.

(9)   Ostrowski, A.; Nordmeyer, D.; Boreham, A.; Brodwolf, R.; Mundhenk, L.; Fluhr, J. W.; Lademann, J.; Graf, C.; Ruhl, E.; Alexiev, U.; Gruber, A. D., Skin barrier disruptions in tape stripped and allergic dermatitis models have no effect on dermal penetration and systemic distribution of AHAPS-functionalized silica nanoparticles. *Nanomedicine* **2014,** *10*, 1571-1581.

(10)   Nabeshi, H.; Yoshikawa, T.; Matsuyama, K.; Nakazato, Y.; Matsuo, K.; Arimori, A.; Isobe, M.; Tochigi, S.; Kondoh, S.; Hirai, T.; Akase, T.; Yamashita, T.; Yamashita, K.; Yoshida, T.; Nagano, K.; Abe, Y.; Yoshioka, Y.; Kamada, H.; Imazawa, T.; Itoh, N.; Nakagawa, S.; Mayumi, T.; Tsunoda, S.; Tsutsumi, Y., Systemic distribution, nuclear entry and cytotoxicity of amorphous nanosilica following topical application. *Biomaterials* **2011,** *32*, 2713-2724.

(11)   Tang, F.; Li, L.; Chen, D., Mesoporous Silica Nanoparticles: Synthesis, Biocompatibility and Drug Delivery. *Adv. Mater.* **2012,** *24*, 1504-1534.

(12)   Wu, S.-H.; Mou, C.-Y.; Lin, H.-P., Synthesis of mesoporous silica nanoparticles. *Chem. Soc. Rev.* **2013,** *42*, 3862-3875.

(13)   Knežević, N. Ž., Core/shell magnetic mesoporous silica nanoparticles with radially oriented wide mesopores. *Process. Appl. Ceram.* **2014,** *8*, 109-112.

(14)   Knezevic, N. Z.; Mrdanovic, J.; Borisev, I.; Milenkovic, S.; Janackovic, D.; Cunin, F.; Djordjevic, A., Hydroxylated fullerene-capped, vinblastine-loaded folic acid-functionalized mesoporous silica nanoparticles for targeted anticancer therapy. *RSC Adv.* **2016,** *6*, 7061-7065.

(15)   Jimenez, C. M.; Knezevic, N. Z.; Rubio, Y. G.; Szunerits, S.; Boukherroub, R.; Teodorescu, F.; Croissant, J. G.; Hocine, O.; Seric, M.; Raehm, L.; Stojanovic, V.; Aggad, D.; Maynadier, M.; Garcia, M.; Gary-Bobo, M.; Durand, J.-O., Nanodiamond-PMO for two-photon PDT and drug delivery. *J. Mater. Chem. B* **2016,** *4*, 5803-5808.

(16)   Knezevic, N. Z.; Mauriello Jimenez, C.; Albino, M.; Vukadinovic, A.; Mrakovic, A.; Illes, E.; Janackovic, D.; Durand, J.-O.; Sangregorio, C.; Peddis, D., Synthesis and Characterization of Core-Shell Magnetic Mesoporous Silica and Organosilica Nanostructures. *MRS Adv.* **2017,** *2*, 1037-1045.

(17)   Croissant, J. G.; Cattoen, X.; Durand, J.-O.; Wong Chi Man, M.; Khashab, N. M., Organosilica hybrid nanomaterials with a high organic content: syntheses and applications of silsesquioxanes. *Nanoscale* **2016,** *8*, 19945-19972.

(18)   Knezevic, N. Z.; Kaluderovic, G. N., Silicon-based nanotheranostics. *Nanoscale* **2017,** *9*, 12821-12829.

(19)   Guan, B.; Cui, Y.; Ren, Z.; Qiao, Z.-a.; Wang, L.; Liu, Y.; Huo, Q., Highly ordered periodic mesoporous organosilica nanoparticles with controllable pore structures. *Nanoscale* **2012,** *4*, 6588-6596.

(20)   Croissant, J. G.; Fatieiev, Y.; Omar, H.; Anjum, D. H.; Gurinov, A.; Lu, J.; Tamanoi, F.; Zink, J. I.; Khashab, N. M., Periodic Mesoporous Organosilica Nanoparticles with Controlled Morphologies and High Drug/Dye Loadings for Multicargo Delivery in Cancer Cells. *Chem. Eur. J.* **2016,** *22*, 9607-9615.

(21)   Schwartz, J. R.; Marsh, R. G.; Draelos, Z. D., Zinc and Skin Health: Overview of Physiology and Pharmacology. *Dermatol. Surg.* **2005,** *31*, 837-847.

(22)   Afonso, S.; Horita, K.; Sousa e Silva, J. P.; Almeida, I. F.; Amaral, M. H.; Lobão, P. A.; Costa, P. C.; Miranda, M. S.; Esteves da Silva, J. C. G.; Sousa Lobo, J. M., Photodegradation of avobenzone: Stabilization effect of antioxidants. *J. Photochem. Photobiol., B* **2014,** *140*, 36-40.

(23)   Ambrogi, V.; Latterini, L.; Marmottini, F.; Pagano, C.; Ricci, M., Mesoporous silicate MCM-41 as a particulate carrier for octyl methoxycinnamate: Sunscreen release and photostability. *J. Pharm. Sci.* **2013,** *102*, 1468-1475.

(24)   Balakrishnan, T.; Ramamurthi, K., Structural, thermal and optical properties of a semiorganic nonlinear optical single crystal: Glycine zinc sulphate. *Spectrochim. Acta, Part A* **2007,** *68*, 360-363.

(25)   Knowles, G. P.; Delaney, S. W.; Chaffee, A. L., Diethylenetriamine[propyl(silyl)]-Functionalized (DT) Mesoporous Silicas as CO_2 Adsorbents. *Industrial & Engineering Chemistry Research* **2006,** *45*, 2626-2633.

(26)   Jaroniec, C. P.; Kruk, M.; Jaroniec, M.; Sayari, A., Tailoring Surface and Structural Properties of MCM-41 Silicas by Bonding Organosilanes. *The Journal of Physical Chemistry B* **1998,** *102* (28), 5503-5510.

(27)   Fatieiev, Y.; Croissant, J. G.; Alamoudi, K.; Khashab, N. M., Cellular Internalization and Biocompatibility of Periodic Mesoporous Organosilica Nanoparticles with Tunable Morphologies: From Nanospheres to Nanowires. *ChemPlusChem* **2017,** *82*, 631-637.

(28)   Wolf, R.; Wolf, D.; Morganti, P.; Ruocco, V., Sunscreens. *Clin. Dermatol.* **2001**, *19*, 452-459.

(29)   Yang, S. I.; Liu, S.; Brooks, G. J.; Lanctot, Y.; Gruber, J. V., Reliable and simple spectrophotometric determination of sun protection factor: A case study using organic UV filter-based sunscreen products. *J Cosmet Dermatol.* **2017** *00*, 1–5. https://doi.org/10.1111/jocd.12390

(30)   Dutra, E. A.; Oliveira, D. A. G. d. C. e.; Kedor-Hackmann, E. R. M.; Santoro, M. I. R. M., Determination of sun protection factor (SPF) of sunscreens by ultraviolet spectrophotometry.   *Rev. Bras. Cienc. Farm.* **2004,** *40*, 381-385.

17

(31)   Sayre, R. M.; Agin, P. P.; LeVee, G. J.; Marlowe, E., A comparison of in vivo and in vitro testing of sunscreening formulas. *Photochem. Photobiol.* **1979,** *29*, 559-566.

(32)   Mukund Manikrao, D.; Sharada Laxman, D., Sunscreens: A review. *Pharmacogn. J.* **2016,** *8*, 171-179.
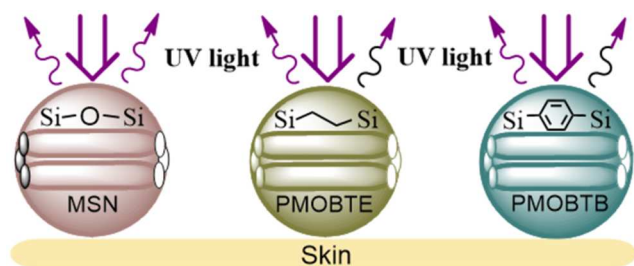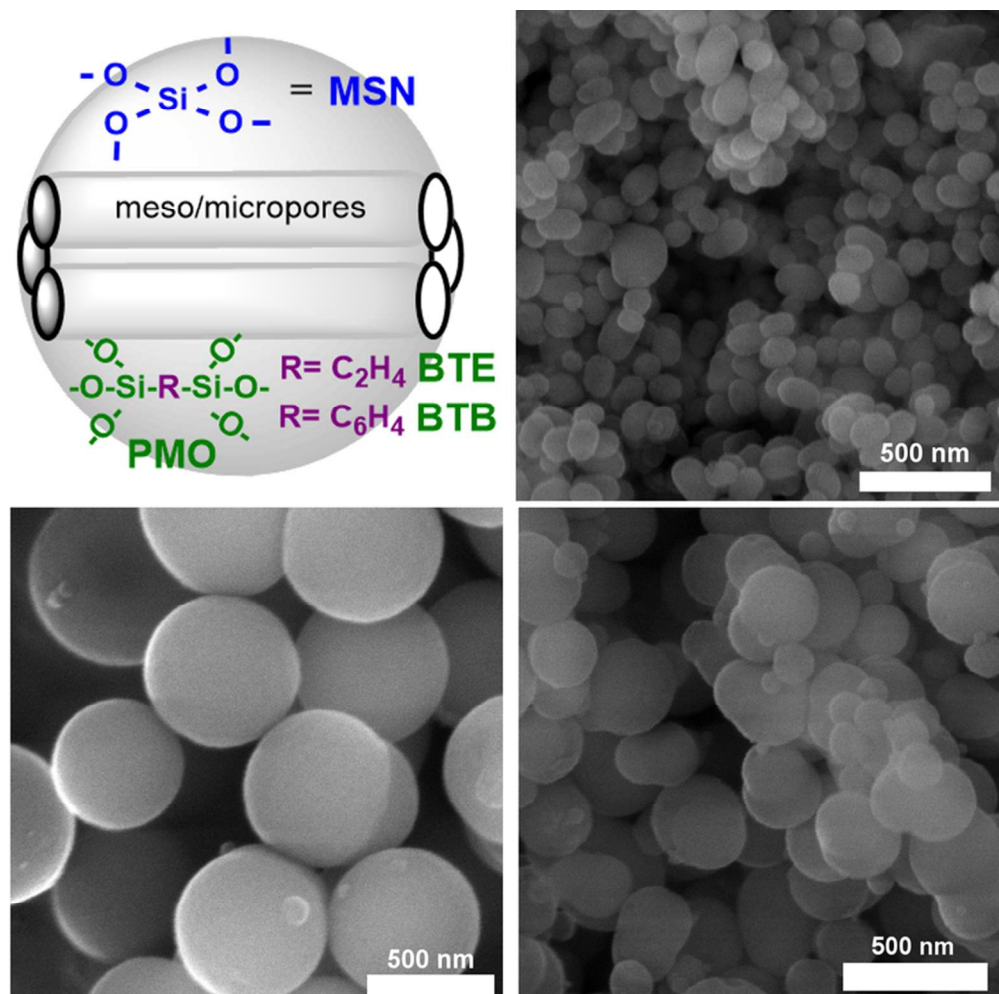
TOC graphic

Table of contents graphic

83x34mm (300 x 300 DPI)

Figure 1. a) Schematic representation of the synthesized MSN and PMO NPs and representative SEM images of MSN (b), PMOBTE (c) and PMOBTB (d).
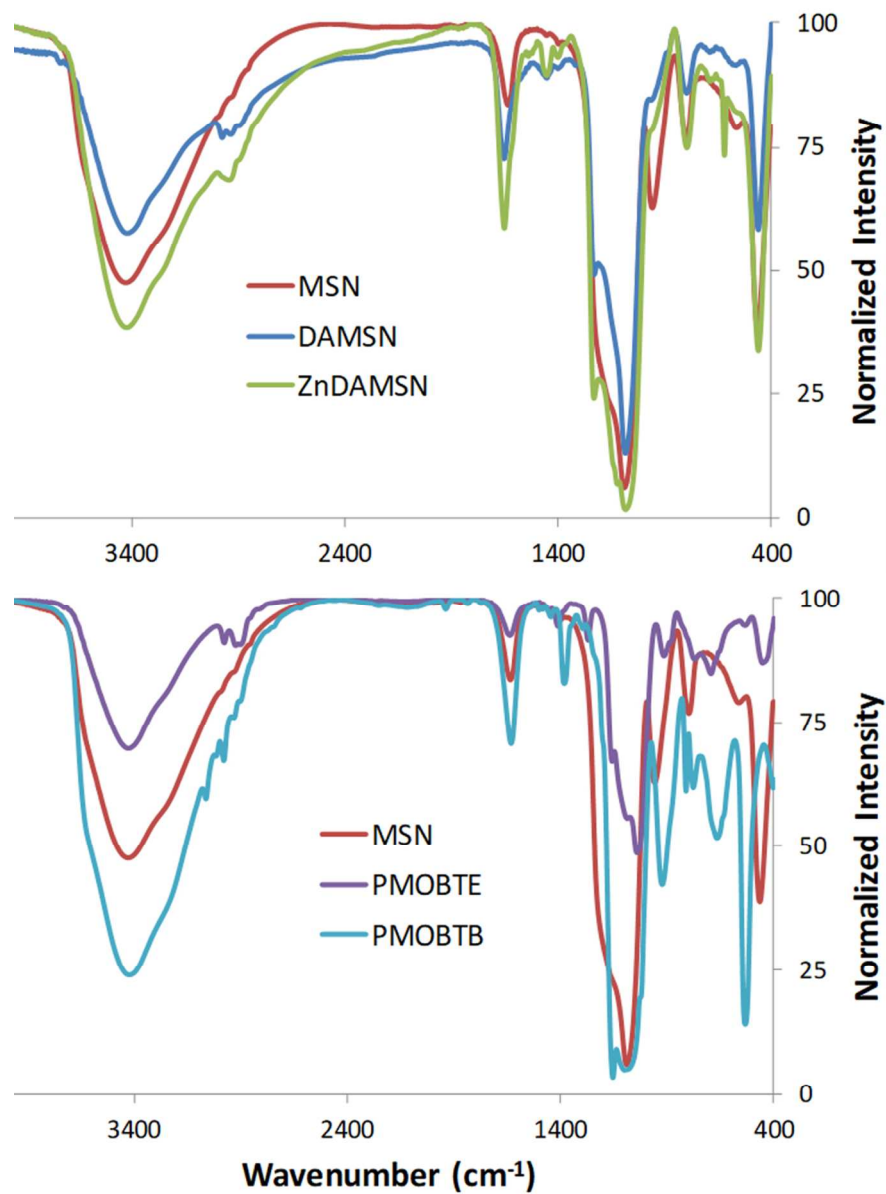
77x77mm (300 x 300 DPI)

Figure 2. Infrared spectra of the synthesized materials: a) Comparison of IR spectra of MSN, DAMSN and ZnDAMSN; b) Comparison of MSN, PMOBTE and PMOBTB
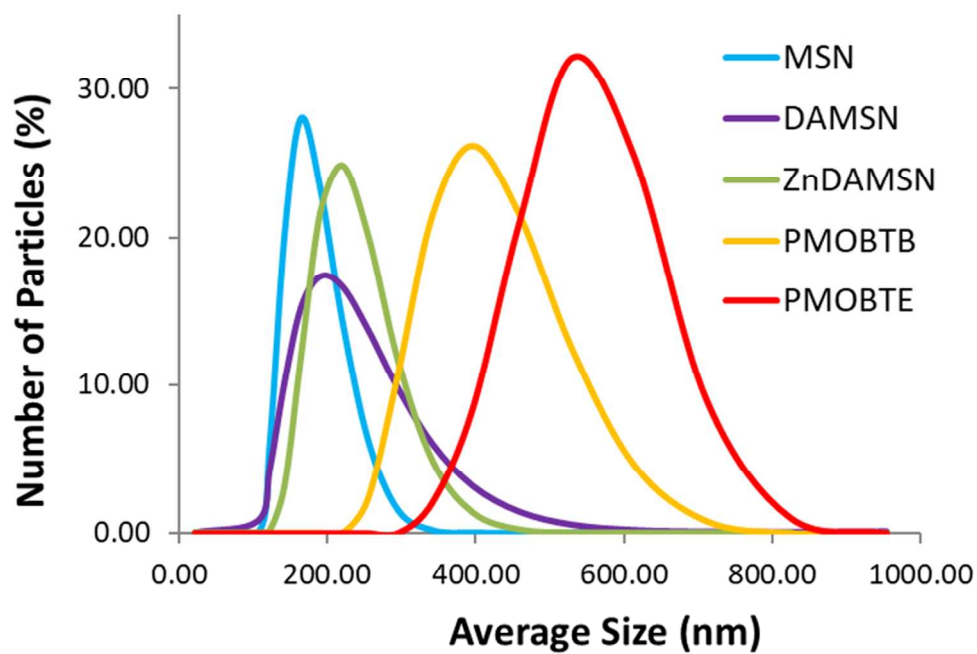
81x110mm (300 x 300 DPI)

1
2
3
4
5
6
7
8
9
10
11
12
13
14
15
16
17
18
19
20
21
22
23
24
25
26
27
28
29
30
31
32
33
34
35
36
37
38
39
40
41
42
43
44
45
46
47
48
49
50
51
52
53
54
55
56
57
58
59
60

Figure 3. Hydrodynamic diameters of nanoparticles as determined by DLS measurements
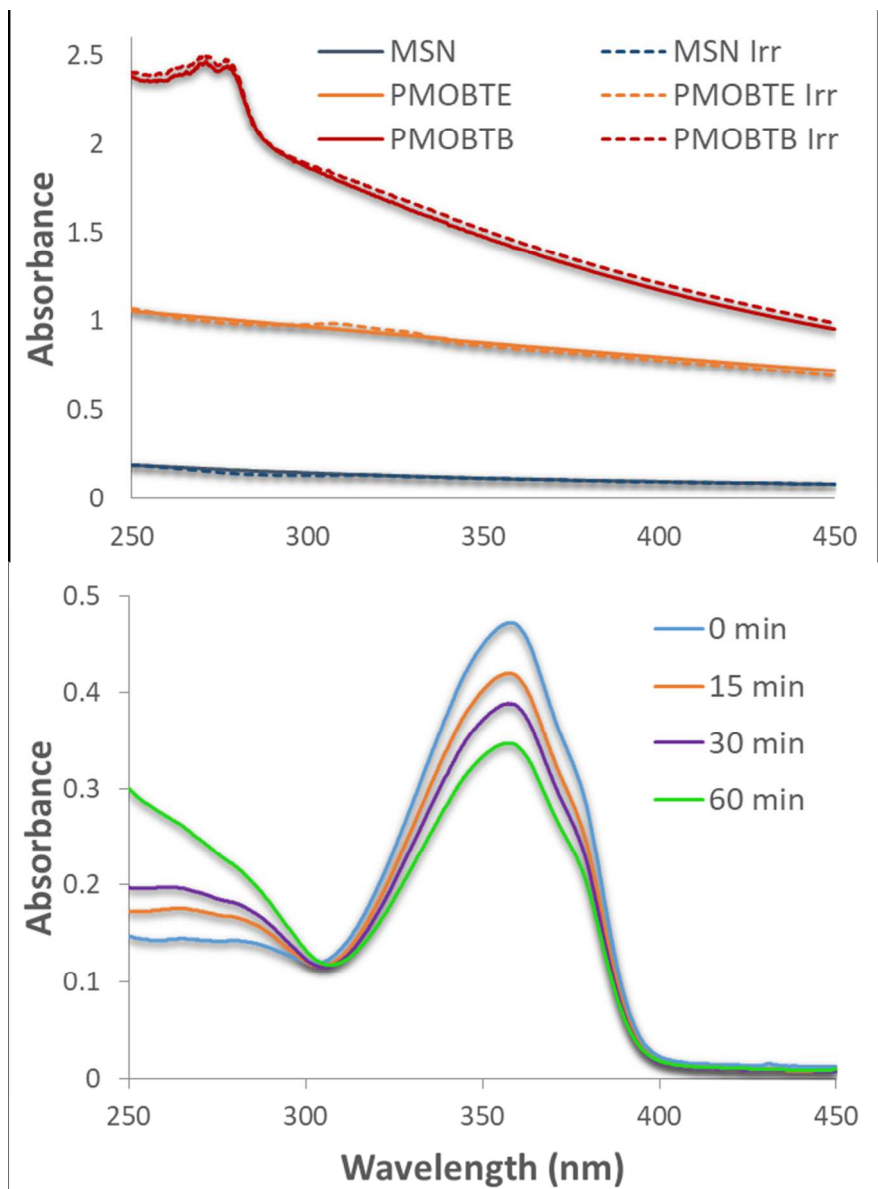
81x55mm (300 x 300 DPI)

Figure 4. UV/VIS spectra of: a) MNS, PMOBTE and PMOBTB in isopropanol before and after exposure to sun-simulated irradiation for 30 minutes (Irr), b) avobenzone in isopropanol upon exposure to irradiation for different time periods.

81x111mm (300 x 300 DPI)